# Adaptive Eco-Driving Strategy and Feasibility Analysis for Electric Trains with On-Board Energy Storage Devices

Chaoxian Wu, Bin Xu, Shaofeng Lu*, Fei Xue, Lin Jiang and Minwu Chen

***Abstract*—With the rapid progress in railway electrification and energy storage technologies, on-board energy storage devices (OESDs) have been widely utilized in modern railway systems to reduce energy consumption. This paper aims to develop the optimal driving strategy of electric trains with three popular types of energy storage devices, namely supercapacitors, flywheels and Li-ion batteries, as the OESD to minimize the net energy consumption. With the given OESD investment cost, the dynamic power limits of different types of OESDs are fully considered to optimize the dynamic discharge/charge behavior of the OESD in the train operation. The case studies investigate the train operation on fully electrified railways, discontinuously electrified railways and catenary-free railways, showing that the optimal eco-driving strategy of the train and discharge/charge behavior of the OESD are significantly different for different type of OESDs. The obtained train speed, OESDs' state of energy (SOE), power profiles and energy-saving potential for each type of OESDs under various scenarios are compared comprehensively, and the results also reveal that the flywheel has the best performance for its energy-saving rate ranging from 0.15 %/k$ to 0.86 %/k$ while Li-ion battery is observed with the weakest performance with energy-saving rate being only 0.01 %/k$ to 0.26 %/k$. The error rate analysis also confirms a satisfactory modeling accuracy of the proposed method.**

This research project is supported and sponsored in part by 2016 NSFC Young Scientist Program Project NO. 61603306 and in part by the Research Development Fund RDF-16-01-42 at Xi'an Jiaotong-Liverpool University and in part by the Fundamental Research Funds for the Central Universities NO. 2020ZYGXZR087 and in part by National Natural Science Foundation of China NO. 51877181 and in part by National Natural Science Foundation of China NO. 51877182.

Chaoxian Wu is with the Shien-Ming Wu School of Intelligent Engineering, South China University of Technology, China, the Department of Electrical Engineering and Electronics, University of Liverpool, UK and the Department of Electrical and Electronic Engineering, Xi'an Jiaotong-Liverpool University, China (Email: Chaoxian.Wu@liverpool.ac.uk)

Bin Xu is with the Department of Electrical and Electronic Engineering, Xi'an Jiaotong-Liverpool University, China and the School of Electrical and Computer Engineering, Cornell University, USA., 14853-5401; (Email: bx83@cornell.edu)

Shaofeng Lu is with the Shien-Ming Wu School of Intelligent Engineering, South China University of Technology, China (Email: lushaofeng@scut.edu.cn)

Fei Xue is with the Department of Electrical and Electronic Engineering, Xi'an Jiaotong-Liverpool University, China, 215123; (Email: Fei.Xue@xjtlu.edu.cn)

Lin Jiang is with the Department of Electrical Engineering and Electronics, University of Liverpool, Liverpool L69 3GJ, U.K. (Email: ljiang@liverpool.ac.uk)

Minwu Chen is with National Rail Transportation Electrification and Automation Engineering Technology Research Center, Chengdu 610031, China and also with the School of Electrical Engineering, Southwest Jiaotong University, Chengdu 610031, China (Email: chenminwu@home.swjtu.edu.cn)

*Corresponding Author: Dr. Shaofeng Lu, Shien-Ming Wu School of Intelligent Engineering, South China University of Technology, China. Phone: +86(0)20-8118-2116. (Email: lushaofeng@scut.edu.cn),

***Index Terms*—Railway transportation, Eco-driving, on-board energy storage device (OESD), Mixed integer linear programming (MILP).**

## NOMENCLATURE

### Parameters

| | |
|---|---|
| $\Delta d_i$ | The $i^{th}$ distance segments $[\mathrm{m}]$ |
| $\eta_k$ | Integrated energy conversion efficiency considering both motor efficiency and internal resistance for k-type OESD |
| $\eta_s$ | Integrated energy conversion efficiency considering both transmission loss and motor efficiency |
| $\overline{a}$ | Preset maximum acceleration rate $[\mathrm{m/s^2}]$ |
| $\overline{F_b}$ | Maximum braking force of train motor $[\mathrm{kN}]$ |
| $\overline{F_t}$ | Maximum traction force of train motor $[\mathrm{kN}]$ |
| $\overline{P_b}$ | Maximum braking power of train motor $[\mathrm{kW}]$ |
| $\overline{P_t}$ | Maximum traction power of train motor $[\mathrm{kW}]$ |
| $\overline{V_i}^2$ | Preset speed limit $[\mathrm{m^2/s^2}]$ |
| $\theta_i$ | Gradient of $\Delta d_i$ |
| $\underline{a}$ | Preset maximum deceleration rate $[\mathrm{m/s^2}]$ |
| $A$ | Davis coefficient $[\mathrm{kN}]$ |
| $B$ | Davis coefficient $[\mathrm{kN \cdot s/m}]$ |
| $b_j^k$ | Coefficient for representing relationship between maximum discharge/charge power and SOE for k-type OESD |
| $C$ | Davis coefficient $[\mathrm{kN \cdot s^2/m^2}]$ |
| $c_j^k$ | Coefficient for representing relationship between maximum discharge/charge power and SOE for k-type OESD |
| $E_{cap}^k$ | Capacity of k-type OESD $[\mathrm{kJ}]$ |
| $g$ | Gravitational constant |
| $i$ | Index of the distance segment |
| $J_j$ | Number of the piece-wise points in SOS2 |
| $k$ | Index of OESD type, $k$=1 represents supercapacitor, $k$=2 represents flywheel and $k$=3 represents Li-ion battery |
| $L$ | A sufficient large number |
| $M_o^k$ | Mass of k-type OESD $[\mathrm{t}]$ |
| $M_t$ | Train mass $[\mathrm{t}]$ |
| $N$ | The number of distance segments of the discretized track |
| $q$ | Moment of inertia of flywheel |
| $SOE_{ini}$ | Preset initial state of energy |
| $T$ | Preset journey time $[\mathrm{s}]$ |

$V_j$ Preset piece-wise speed point for speed-related variables linearization $[\mathrm{m/s}]$
$V_{ini}$ Preset initial train speed $[\mathrm{m/s}]$
$V_{ter}$ Preset terminal train speed $[\mathrm{m/s}]$
$Y_j^{k,ch}$ Preset piece-wise point for product linearization on charge process
$Y_j^{k,dch}$ Preset piece-wise point for product linearization on discharge process

**Variables**

$\alpha_{i,j}^{v}$ SOS2 variables for speed-related variables linearization
$\alpha_{i,j}^{k,ch}$ SOS2 variables for product linearization on charge process of k-type OESD
$\alpha_{i,j}^{k,dch}$ SOS2 variables for product linearization on discharge process of k-type OESD
$\beta_{i,j}^{v}$ SOS2 variables for speed-related variables linearization
$\beta_{i,j}^{k,ch}$ SOS2 variables for product linearization on charge process of k-type OESD
$\beta_{i,j}^{k,dch}$ SOS2 variables for product linearization on discharge process of k-type OESD
$\lambda_i$ 0-1 variables to determine the train operation mode in $\Delta d_i$
$\mu_{i,j}^{k,ch_\alpha}$ 0-1 variables for product linearization on charge process of k-type OESD
$\mu_{i,j}^{k,ch_\beta}$ 0-1 variables for product linearization on charge process of k-type OESD
$\mu_{i,j}^{k,dch_\alpha}$ 0-1 variables for product linearization on discharge process of k-type OESD
$\mu_{i,j}^{k,dch_\beta}$ 0-1 variables for product linearization on discharge process of k-type OESD
$\mu_{i,j}^{v,\alpha}$ SOS2 variables for speed-related variables linearization
$\mu_{i,j}^{v,\beta}$ 0-1 variables for speed-related variables linearization
$E_{i,r}$ Energy transmitted to OESD from motor $[\mathrm{kJ}]$
$E_{i,s}$ Energy from substation $[\mathrm{kJ}]$
$E_{i,ch}^{k}$ Energy charged to k-type OESD $[\mathrm{kJ}]$
$E_{i,dch}^{k}$ Energy discharged from k-type OESD $[\mathrm{kJ}]$
$u_j^k$ 0-1 variables for piece-wise linearization of the relationship between maximum discharge/charge power and SOE for k-type OESD
$v_i^2$ Square of train speed when train reaches $\sum_1^{i-1}\Delta d_i$ $[\mathrm{m^2/s^2}]$

## I. Introduction

In modern society, railway systems have become one of the important transportation modes worldwide. Due to the growing travel demands, the global railway networks produce 336 million tons of carbon dioxide emissions and consume 200 million joules of energy per year [1]. In order to cope with the increasing resource consumption of the railway systems, reducing their energy consumption has become an important topic. As an emerging technology, on-board energy storage devices (OESDs) and stationary energy storage systems have been utilized in many modern railway systems to save energy consumption as well as to reduce their carbon emissions [2]–[5].

Three types of OESDs are commonly utilized in electrified railway systems, namely supercapacitors, flywheels and electrochemical batteries. Supercapacitors are widely utilized as the OESD, for example in many urban rail transit systems have been equipped with them, such as tram lines [6], metro lines [7] in Brussels, Madrid metro line [8], Blackpool tramway [9], Mannheim tramway [10] and Paris tram line [11]. For the flywheel, early in 1988 it has been proposed as an OESD for trains to avoid regenerative braking cancellation and to compensate for voltage drops. However, till now the flywheel as OESD is still at the early development stage [3], and they are only studied in heavy haul trains [12] and in light rail vehicles [13] in academic papers. In 2006, the first Li-ion battery was installed on the train of the West Japan Railway [14] and it is also used in Sapporo Li-ion battery-driven light rail [15]. Besides, other types of electrochemical battery has also been applied as OESD in railway systems, for instance, Ni-MH battery-driven Catadis tramway is already in operation in Nice, France [16].

With the fast development of the energy storage technologies and the increasing utilization of the OESD in modern railway systems, the research to consider both the train operation and the OESD is becoming hot topic in recent years. One of the research direction is to design the optimal control and discharge/charge strategy of the OESD by considering the practical train operation. In [17] a fast-swap charging (FSC) is introduced to control the empty energy storage components to be charged at low electricity-demand periods in a light rail systems equipped with on-board supercapacitors to save the average operating cost. Zhong *et al.* [18] propose an on-board supercapacitor control strategy based on the train electric braking characteristics to absorb as much regenerative energy as possible. Based on the power slit information from the catenary-free tram system, an optimal integration strategy for the correct size of on-board supercapacitors and the power of the inductive energy transfer are proposed to cut the system's power consumption [19]. Focusing on the metro systems, a mathematical-programming-based approach is proposed to determine the optimal size and control strategy of supercapacitors, flywheels and Li-ion batteries based on the real train speed data in [20]. Apart from being used in the metro systems and trams in the city, a supercapacitor-based storage system integrated at the high-speed railway to recover the regenerative energy of the trains based on the master-slave control strategy is reported in [21].

However, many researchers realize that only optimizing the OESD control strategy based on the preset train operation data might lead to a suboptimal solution since the train operation is not optimized simultaneously. As a result, the integrated optimization of both the train operation and OESD control strategy is necessary to further reduce energy consumption. Based on dynamic programming (DP), the optimal train speed with supercapacitor as OESD are found [22], [23]. By modeling the circuits of the supercapacitor, both papers have demonstrated the feasibility to identify the optimal train speed profiles. Huang *et al.* [24] also employs DP to explore the

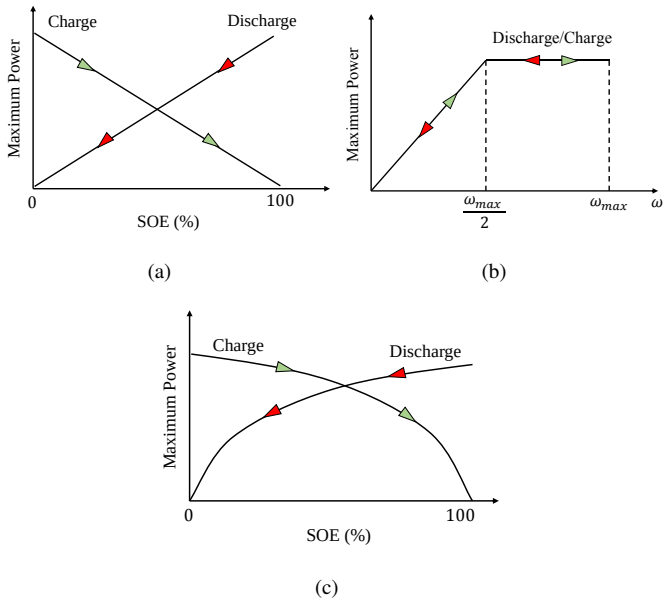


Fig. 1. The illustration of the maximum discharge/charge power for (a) supercapacitors, (b) flywheels and (c) Li-ion batteries. **For the supercapacitor**, the maximum discharge/charge power limit of it has linear relationship with its real-time energy status, namely state of energy (SOE), where the maximum discharge power decreases linearly from SOE being 100% to 0 and maximum charge power also decreases linearly from SOE being 0 to 100% [29], [30]. **As for the flywheel**, its maximum discharge/charge power increase linearly with its angular speed $\omega$ until $\omega$ reaches the half of the maximum angular speed $\omega_{max}$ then becomes a constant value [31], [32]. **For the electrochemical batteries**, such as lead-acid batteries, Ni-Cd batteries, NiMH batteries, Li-ion batteries and so on, the dynamic power limits of them is also related to its real-time SOE, where the maximum discharge power decreases with an increasing gradient from SOE being 100% to 0 and its maximum charge power decreases with an increasing gradient from SOE being 0 to 100% [33]–[35]

energy-saving potential of supercapacitor by optimizing the train speed profiles. A general integrated optimization model for trains with a general model of OESD is proposed by Wu *et al.* [25] with high energy-saving rate and computational efficiency. The work is extended in [26] and the speed profiles optimization problem for two inter-station sections are studied with the consideration of the charge/discharge control at the intermediate station. Based on the industrial information, the speed profile optimization problem for catenary-free train with Li-ion batteries is considered in [27], where a battery-driven train designed by Bombardier Transportation and tested in UK is studied. In [28], the optimal power split and speed profiles of the caternary-free tram equipped with suprecapacitor are found by utilizing DP as well.

In fact, the discharge/charge process of different types of OESD is strongly shaped by their own dynamic power limits which is related to their current status [36]. Figure 1 shows the dynamic power limits of the three main types of OESD. It can be noted that the discharge/charge power limits of different types of OESD are closely related to their energy status (for supercapacitors and electrochemical batteries) or motion status (for flywheels), but few reports can be found in the literature. In the above literature review it can be seen that train operation problem with supercapacitors as OESD have been studied by some researchers [22]–[28] while flywheels and electrochemical batteries are still rarely investigated. A systematic study and comparison on the influence of different types of energy storage devices on the train operation and its comparison is still missing in the literature. Also, in the existing works the dynamic discharge/charge characteristics of the OESD are not considered, which undermines the model's applicability in the real world. Since these dynamic discharge/charge power limits may have further influences on the train operation and result in different control strategies for both train and OESD, a systematic investigation is needed. In this case, this paper aims to develop a new mixed integer linear programming (MILP) model to find the optimal driving strategy, namely the speed profile, of the train equipped with three popular types of OESDs, i.e. supercapacitor, flywheel and Li-ion battery to minimize the net energy consumption by taking into account their corresponding dynamic discharge/charge limits. The contributions of the paper are outlined as follows:

- This paper provides a comprehensive comparative study on the energy-saving performance of three popular types of OESD considering the investment constraints and dynamic power limits using the proposed MILP model.
- The optimal driving strategy of the train and the discharge/charge behavior for three types of OESDs are located, where the corresponding train speed, SOE and power of OESD are all obtained.
- The optimal eco-driving strategies on fully electrified railways, discontinuously electrified railways and catenary-free railways are found, and insightful comparisons of the energy-saving and feasibility of different types of OESD are given.

It is noted that the main purpose of the proposed method is to obtain the optimal train speed profile and OESD discharge/charge strategy considering the dynamic relationship between OESD instant power and its SOE, other operational factors such as variations of peak power capacities and their impacts on cycling life time of the OESD are not within the scope of the research.

The remainder of the paper is organized as follows: Section II presents the details of the model formulation, covering the train movement modeling, energy flow modeling and the dynamic discharge/charge behavior modeling. Section III elaborates on the solution approach to integrate each components in the model by using MILP, where the constraints and objective of the model are given. Section IV covers a case study and a detailed comparative study on different operation scenarios, and the error analysis related to the proposed approach is discussed. Section V draws the conclusion of the research.

## II. Model Formulation

In this section, the mathematical modeling of the train movement, energy flow and dynamic discharge/charge power limit of different types of OESD are elaborated.

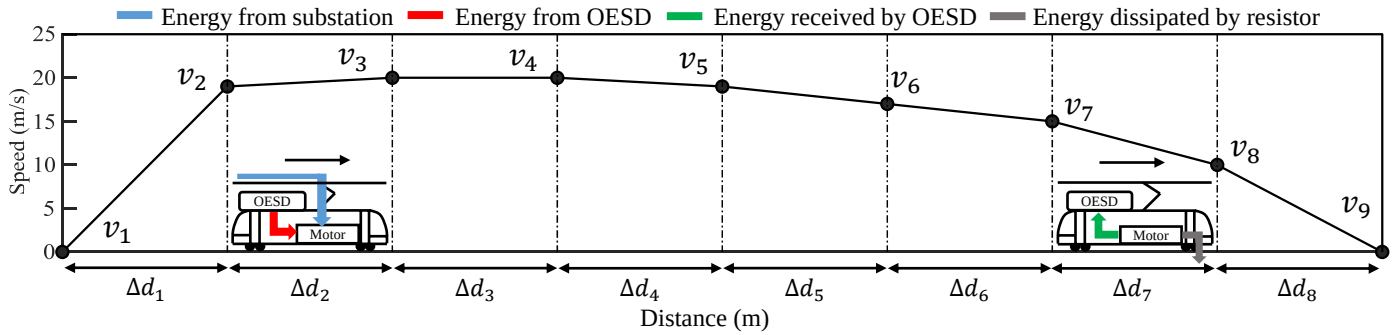


Fig. 2. A schematic of the speed profile and energy flow of the train with OESD on a discretized track. The number of $\Delta d_i$, denoted by $N$, is 8 thus there are 9 $v_i$ in total.

### A. Modeling the Train Movement and Energy Transmission

Similar to the model first proposed in [25], the track length $D$ between two adjacent stations is divided into $N$ segments, as the $\Delta d_i$ shown in Figure 2. As a result, there are $N+1$ speed points $v_i$ in total. In the model, the train is assumed to do uniformly accelerated/decelerated motion in each $\Delta d_i$. The track length $D$ can be equally divided or unequally divided according to the real route conditions e.g. gradients and speed limits. As a result, the acceleration/deceleration $a_i$ in $\Delta d_i$ can be expressed by (1).

$$a_i = \pm \frac{v_{i+1}^2 - v_i^2}{2\Delta d_i} \tag{1}$$

Here the positive value of $a_i$ implies the acceleration and negative value implies the deceleration.

For each $\Delta d_i$, the average speed $v_{i,ave}$ can be calculated by using (2).

$$v_{i,ave} = \frac{v_i + v_{i+1}}{2} \tag{2}$$

Thus, the elapsed time $\Delta t_i$ for each $\Delta d_i$ is shown in (61).

$$\Delta t_i = \frac{\Delta d_i}{v_{i,ave}} \tag{3}$$

The kinetic energy change of the train $E_{i,v}$ in each $\Delta d_i$ can be expressed in (4).

$$E_{i,v} = \frac{1}{2}(M_t + M_o^k)(v_{i+1}^2 - v_i^2) \tag{4}$$

When the train is running on the track, it is imposed with drag force $F_{i,drag}$ in each $\Delta d_i$ estimated by the Davis Equation shown in (5).

$$F_{i,drag} = A + Bv_{i,ave} + Cv_{i,ave}^2 \tag{5}$$

As a result, the work of the drag force $E_{i,f}$ can be obtained in each $\Delta d_i$ as shown in (6).

$$E_{i,f} = F_{i,drag}\Delta d_i \tag{6}$$

In addition, since there are varied gradients along with the track, the work of the gravity $E_{i,p}$, which is also the potential change of the train, caused by gravity is applied to the train. Thus, in each $\Delta d_i$, it can be obtained as shown in (7).

$$E_{i,p} = (M_t + M_o^k) g \Delta d_i \theta_i \tag{7}$$

where positive value of $\theta_i$ represents the down-slope, and negative one represents the up-slope.

During the journey, the train can consume the energy from the substation $E_{i,s}$ and energy discharged by the OESD $E_{i,dch}^k$ when the train is motoring. Here the force of the train motor produces can be expressed in (8).

$$E_{i,m} = E_{i,s}\eta_s + E_{i,dch}^k \eta_k \tag{8}$$

When the train is braking, the motor is in regenerative braking mode and part of the energy can be delivered to the OESD, which is denoted as $E_{i,r}$ here. Thus, the energy that can be charged to OESD, demoted as $E_{i,ch}^k$, is represented in (9).

$$E_{i,r} = -\frac{E_{i,ch}^k}{\eta_k} \tag{9}$$

Since the the motor has its own traction/braking characteristics, thus, in each $\Delta d_i$, the maximum force the motor can conduct should follow the limitation of its maximum traction force $\overline{F_t}$ and maximum braking force $\overline{F_b}$. Also, it needs to be limited by the maximum traction power $\overline{P_t}$ and maximum braking power $\overline{P_b}$. Thus, these can be expressed as shown in (10) and (11).

$$\overline{E_{i,t}^F} = \overline{F_t}\Delta d_i, \quad \overline{E_{i,b}^F} = \overline{F_b}\Delta d_i \tag{10}$$

$$\overline{E_{i,t}^P} = \overline{P_t}\Delta t_i, \quad \overline{E_{i,b}^P} = \overline{P_b}\Delta t_i \tag{11}$$

where $\overline{E_{i,t}^F}$, $\overline{E_{i,b}^F}$, $\overline{E_{i,t}^P}$ and $\overline{E_{i,b}^P}$ are the maximum force that the motor can produce in $\Delta d_i$ limited by the maximum traction/braking force and power respectively.

### B. Dynamic Discharge/Charge Power Limits of OESD

In the paper, three different types of energy storage devices, namely the supercapacitor, flywheel and Li-ion battery as OESD are modeled. From [37]–[39], the energy and power density and capital cost of each type of OESD can be obtained, as shown in Table I. From Table I the average capital cost of three OESD types can be calculated to be 200 $/kW for supercapacitor, 300 $/kW for flywheel and 1875 $/kW for Li-ion battery respectively. For making a general comparison, a constant investment for each OESD is set to be 150 k$. As

TABLE I
THE ENERGY DENSITY PER UNIT MASS/VOLUME, POWER DENSITY PER UNIT MASS AND CAPITAL COST PER UNIT POWER CAPACITY FOR THREE TYPES OF OESD [37]–[39]

| OESD type | Energy density | | Power density | Capital cost |
|---|---|---|---|---|
| | (kWh/t) | (kWh/m$^3$) | (kW/t) | ($/kW) |
| Supercapacitor | 2.5-15 | 10-30 | 500-5000 | 100-300 |
| Flywheel | 5-100 | 20-80 | 1000-5000 | 250-350 |
| Li-ion battery | 75-200 | 150-500 | 100-350 | 1200-4000 |

TABLE II
THE MAXIMUM POWER, CAPACITY AND WEIGHT OF THE ADOPTED OESD WITH AN INVESTMENT OF 150 K$

| OESD type | Maximum power (kW) | Capacity (kWh) | Mass (t) |
|---|---|---|---|
| Supercapaitor | 750 | 1.87 | 0.85 |
| Flywheel | 500 | 3.50 | 0.50 |
| Li-ion battery | 80 | 13.88 | 0.08 |

a result, the maximum power of each OESD can be obtained and shown in Table II, where the capacity and mass for OESD with corresponding maximum power are also tabulated. In this paper, the listed OESD will be adopted for our case study.

As shown in Figure 1, the dynamic discharge/charge power limits of the OESD is mainly determined by its current SOE and motion status during the whole journey. There are $n+1$ $SOE_i^k$ during the journey with $n$ $\Delta d_i$. SOE for k-type OESD when the train passes $\Delta d_i$, denoted as $SOE_{i+1}^k$, can be expressed in (12).

$$SOE_{i+1}^k = SOE_1^k + \frac{-\sum_1^i E_{i,dch}^k + \sum_1^i E_{i,ch}^k}{E_{cap}^k} \times 100\% \quad (12)$$

where $SOE_1^k$ is the initial stored energy in $k$-type OESD.

*1) Supercapacitor:*

For supercapacitor, from [29], [30] it is shown that the empirical real-time maximum power and SOE is linear correlated, as shown in Figure 3. The maximum discharge power and the maximum charge power for each $\Delta d_i$, denoted as $\overline{P_{i,dch}^1}$ and $\overline{P_{i,ch}^1}$, can be expressed by (13) and (14).

$$\overline{P_{i,dch}^1} = c_1^1 SOE_i^1 + b_1^1 \quad (13)$$

$$\overline{P_{i,ch}^1} = c_2^1 SOE_i^1 + b_2^1 \quad (14)$$

*2) Flywheel:*

For flywheel, since it is known from [31], [32] that in theory its maximum discharge/charge power increase linearly with its angular speed $\omega$ until it reaches the half of the maximum angular speed $\omega_{max}$, then it becomes a constant value. Thus, in each $\Delta d_i$, the relationship between flywheel's maximum discharge/charge power $\overline{P_{i,dch}^2}/\overline{P_{i,ch}^2}$ and its current angular speed $\omega_i$ can be shown in (15).

$$\overline{P_{i,dch}^2} = \overline{P_{i,ch}^2} = \begin{cases} c\omega_i & 0 \le \omega_i \le \frac{1}{2}\omega_{max} \\ \frac{c\omega_{max}}{2} & \frac{1}{2}\omega_{max} \le \omega_i \le \omega_{max} \end{cases} \quad (15)$$

where $c$ is the parameter for the linear relationship before the $\omega_i$ reaches $\frac{1}{2}\omega_{max}$.

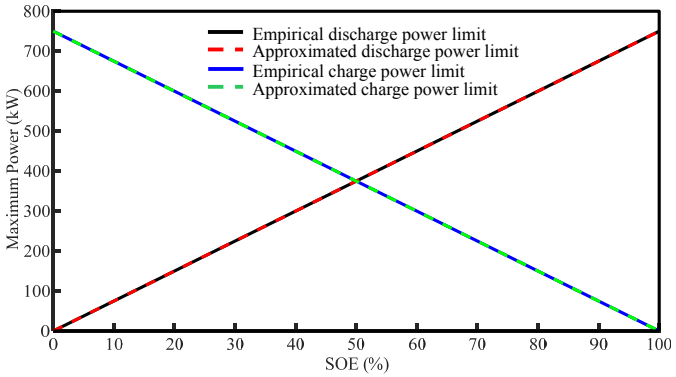


Fig. 3. The empirical and linear approximation of the relationship between the power limits and SOE of the adopted supercapacitor, where the maximum power is 750 kW for both discharge and charge and power limits change linearly with respect to SOE.

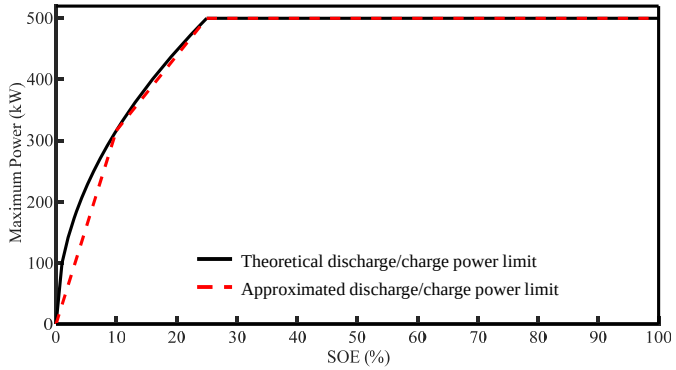


Fig. 4. The theoretical and linear approximation of the relationship between the power limits and SOE of the adopted flywheel, where the maximum power is 500 kW for both discharge and charge and power limit is pieced into 3 linear sections with respect to SOE.

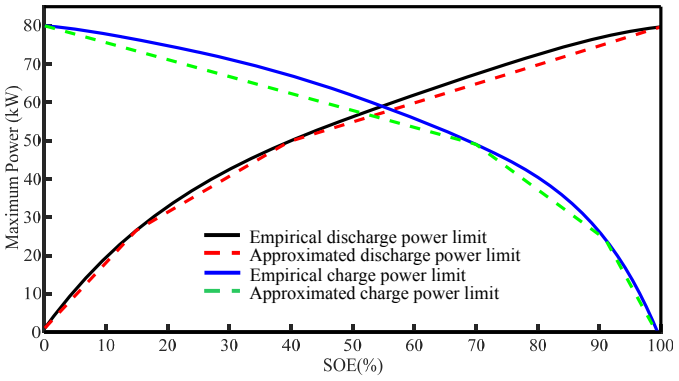


Fig. 5. The empirical and linear approximation of the relationship between the power limits and SOE of the adopted Li-ion battery, where the maximum power is 80 kW for both discharge and charge and power limits are pieced into 3 linear sections with respect to SOE respectively.

Since the flywheel transforms the electrical energy to kinetic energy, the real-time energy status can be expressed by using (16).

$$SOE_i^2 E_{cap}^2 = \frac{1}{2} M_o^2 q \omega_i^2 \quad (16)$$

TABLE III
THE PARAMETER $(c_j^k, b_j^k)$ CALIBRATION OF THE APPROXIMATION FOR THREE TYPES OF OESD ADOPTED IN THIS PAPER

| Piece-wise section | Discharge | | |
|---|---|---|---|
| | Supercapacitor | Flywheel | Li-ion battery |
| 1 | (7.5, 0) | (31.62, 0) | (1.768, 0) |
| 2 | / | (12.25, 193.67) | (0.93, 12.58) |
| 3 | / | (0, 500) | (0.50, 29.58) |
| | Charge | | |
| 1 | (-7.5, 750) | (31.62, 0) | (-0.44, 80) |
| 2 | / | (12.25, 193.67) | (-1.24, 135.85) |
| 3 | / | (0, 500) | (-2.425, 242.5) |

Thus, the relationship between the discharging/charging power limits of flywheel and its SOE can be established in (17).

$$\overline{P_{i,dch}^2} = \overline{P_{i,ch}^2} = \begin{cases} c\sqrt{\frac{2\times SOE_i^2 E_{cap}^2}{M_o^2 q}} & 0 \le SOE_i^2 \le 25\% \\ \frac{c\omega_{max}}{2} & 25\% \le SOE_i^2 \le 100\% \end{cases} \tag{17}$$

It can be easily observed that when the flywheel stores one-fourth the maximum capacity, it would reach the maximum discharging/charging power limitations, as illustrated in Figure 4.

To approximate this relationship, the curve is pieced into 3 parts, a shown in Figure 4, where the division points are chosen to be $SOE_i^2 = 10\%$ and $SOE_i^2 = 25\%$. As a result, (17) can be reformulated in (18).

$$\overline{P_{i,dch}^2} = \overline{P_{i,ch}^2} = \begin{cases} c_1^2 SOE_i^2 + b_1^2 & 0 \le SOE_i^2 \le 10\% \\ c_2^2 SOE_i^2 + b_2^2 & 10\% \le SOE_i^2 \le 25\% \\ c_3^2 SOE_i^2 + b_3^2 & 25\% \le SOE_i^2 \le 100\% \end{cases} \tag{18}$$

*3) Li-ion Battery:*

According to [33]–[35], it is shown that Li-ion batteries' discharge/charge power limits are related to its current SOE as well, but it performs quite differently with the supercapacitors and flywheels, where the charge power limit decreases when SOE increases while its discharge power limit decreases as SOE decreases. This relationship of the adopted Li-ion battery of the paper is shown in Figure 5. To model this feature with the approximation, similar as the flywheel, the dynamic power limits for both discharge and charge process, $\overline{P_{i,dch}^3}$ and $\overline{P_{i,ch}^3}$, are segmented into 3 parts respectively, and the formulations of which are shown in (19) and (20).

$$\overline{P_{i,dch}^3} = \begin{cases} c_1^3 SOE_i^3 + b_1^3 & 0 \le SOE_i^3 \le 15\% \\ c_2^3 SOE_i^3 + b_2^3 & 15\% \le SOE_i^3 \le 40\% \\ c_3^3 SOE_i^3 + b_3^3 & 40\% \le SOE_i^3 \le 100\% \end{cases} \tag{19}$$

$$\overline{P_{i,ch}^3} = \begin{cases} c_4^3 SOE_i^3 + b_4^3 & 0 \le SOE_i^3 \le 70\% \\ c_5^3 SOE_i^3 + b_5^3 & 70\% \le SOE_i^3 \le 90\% \\ c_6^3 SOE_i^3 + b_6^3 & 90\% \le SOE_i^3 \le 100\% \end{cases} \tag{20}$$

From the above modeling process, it can be seen that the parameters for the linear approximation of the power limits curve needs to be calibrated, especially for flywheel and Li-ion battery, and the results of which are tabulated in Table III.

## III. SOLUTION APPROACH - MILP

To construct a linear programming problem, the relationships among each variables should be linear. In this section, the piece-wise linear method is utilized to conduct the linearization of the nonlinear relationships in the proposed model. In addition, the logical integer variables are introduced into the model to help control the nonlinear decision making process in the method. The decision variables, constraints and objective of the model adjusted into a MILP problem are given followed.

### A. Speed-related Variables Linearization

It can be seen that the relationship among the speed-related variables, $v_i$, $v_i^2$, $v_{i,ave}^2$ and $\frac{1}{v_{i,ave}}$, are not linear. As a result, a series of special ordered set type 2 (SOS2), among which only two adjacent ones can be greater than 0 with the total sum of all variables equal to 1 [40], is used for linearization. To linearize this relationship, the value range is divided into $J_1$ sections and a series of piece-wise linear section points are chosen to represent the speed within the range from $V_1$ to $V_{J_1}$, as discussed in [25]. In this case, two sets of SOS2 are applied in linearizing the speed-related relationships, as shown in (21) - (23).

$$v_i^2 = \sum_{j=1}^{J_1} V_j^2 \alpha_{i,j}^v, \quad v_i^{'} = \sum_{j=1}^{J_1} V_j \alpha_{i,j}^v \tag{21}$$

$$v_{i,ave}^{'} = \frac{v_i^{'} + v_{i+1}^{'}}{2} = \sum_{j=1}^{J_1} V_j \beta_{i,j}^v \tag{22}$$

$$v_{i,ave}^{'2} = \sum_{j=1}^{J_1} V_j^2 \beta_{i,j}^v, \quad \frac{1}{v_{i,ave}^{'}} = \sum_{j=1}^{J_1} \frac{1}{V_j} \beta_{i,j}^v \tag{23}$$

$\alpha_{i,j}^v$ and $\beta_{i,j}^v$ are two sets of SOS2 to linearize the speed-related variables above. Thus, the SOS2 series need to satisfy (24) and (25).

$$\sum_{j=1}^{J_1} \alpha_{i,j}^v = 1, \quad \sum_{j=1}^{J_1} \beta_{i,j}^v = 1 \tag{24}$$

$$0 \le \alpha_{i,j}^v \le 1, \quad 0 \le \beta_{i,j}^v \le 1 \tag{25}$$

To ensure that only the adjacent $\alpha_{i,j}^{v,\alpha}$ and $\beta_{i,j}^{v,\beta}$ can be nonzero and their sum being 1, 0-1 control variables $\mu_{i,j}^v$ need to be imposed, as shown in (26) to (27).

$$\alpha_{i,j}^v + \alpha_{i,j+1}^v - \mu_{i,j}^{v,\alpha} \ge 0, \quad \beta_{i,j}^v + \beta_{i,j+1}^v - \mu_{i,j}^{v,\beta} \ge 0 \tag{26}$$

$$\sum_{j=1}^{J_1-1} \mu_{i,j}^{v,\alpha} = 1, \quad \sum_{j=1}^{J_1-1} \mu_{i,j}^{v,\beta} = 1 \tag{27}$$

### B. Determination of Train Operation Mode

Since the train cannot conduct traction and braking at the same time, the traction energy in (8) and regenerative energy in (9) of the train cannot exist simultaneously in one $\Delta d_i$. In this case, the 0-1 variables $\lambda_i$ need to be imposed into the

model to determine the train operation mode in each $\Delta d_i$, as shown in (28) - (29).

$$0 \le E_{i,s} \le \lambda_i L, \quad 0 \le E^k_{i,dch} \le \lambda_i L \tag{28}$$

$$0 \le E^k_{i,ch} \le (1-\lambda_i) L \tag{29}$$

It can be seen that when $\lambda_i$ is 1, the train is in traction mode and the OESD and substation can supply the train together. In contrast, when $\lambda_i$ is 0, the train is braking and the OESD can be charged to recover the regenerative energy.

### C. Linearization on OESD Dynamic Power Limits

As in Section II-B the dynamic discharging/charging characteristics of three types of OESD, supercapacitor, flywheel and Li-ion battery, have been constructed and elaborated, this section is aimed at discussing the linearization of the relevant relationships among variables by using SOS2 as well as the integer logical variables.

In (18), the relationship between the power limits and SOE of the flywheel has been formulated into a piece-wise function with 3 parts. To control the SOE in each piece-wise part, in each $\Delta d_i$, integer logical variables are imposed to linearize these functions, as shown in (30) - (32).

$$\begin{aligned}\overline{P^2_{i,dch}} = \overline{P^2_{i,ch}} = {} & c_1^2 SOE^2_{i,1} + b_1^2 u^2_{i,1} + c_2^2 SOE^2_{i,2} + b_2^2 u^2_{i,2} \\ & + c_3^2 SOE^2_i + b_3^2 u^2_{i,3}\end{aligned} \tag{30}$$

$$\begin{cases} 0 \le SOE^2_{i,1} \le 10\% u^2_{i,1}, \\ 10\% u^2_{i,2} \le SOE^2_{i,2} \le 25\% u^2_{i,2}, \\ 25\% u^2_{i,3} \le SOE^2_{i,3} \le 100\% u^2_{i,3} \end{cases} \tag{31}$$

$$u^2_{i,1} + u^2_{i,2} + u^2_{i,3} = 1 \tag{32}$$

where $SOE^2_{i,1}$, $SOE^2_{i,2}$ and $SOE^2_{i,3}$ are the auxiliary variables to represent the $SOE^2_i$ in 3 piece-wise sections.

In (19) and (20), the relationships between the discharging/charging power limits and SOE of the Li-ion battery has been formulated into a piece-wise function with 3 parts respectively. Similarly, to control the SOE in each piece-wise part, in each $\Delta d_i$, integer logical variables are imposed to linearize these functions, as shown in (33) - (38) for discharging power limits.

$$\begin{aligned}\overline{P^3_{i,dch}} = {} & c_1^3 SOE^3_{i,1} + b_1^3 u^3_{i,1} + c_2^3 SOE^3_{i,2} + b_2^3 u^3_{i,2} \\ & + c_3^3 SOE^3_{i,3} + b_2^3 u^3_{i,3}\end{aligned} \tag{33}$$

$$\begin{aligned}\overline{P^3_{i,ch}} = {} & c_4^3 SOE^3_{i,4} + b_4^3 u^3_{i,4} + c_5^3 SOE^3_{i,5} + b_5^3 u^3_{i,5} \\ & + c_6^3 SOE^3_{i,6} + b_6^3 u^3_{i,6}\end{aligned} \tag{34}$$

$$\begin{cases} 0 \le SOE^3_{i,1} \le 15\% u^3_{i,1}, \\ 15\% u^3_{i,2} \le SOE^3_{i,2} \le 40\% u^3_{i,2}, \\ 40\% u^3_{i,3} \le SOE^2_{i,3} \le 100\% u^3_{i,3} \end{cases} \tag{35}$$

$$\begin{cases} 0 \le SOE^3_{i,4} \le 70\% u^3_{i,4}, \\ 70\% u^3_{i,4} \le SOE^3_{i,4} \le 90\% u^3_{i,4}, \\ 90\% u^3_{i,5} \le SOE^2_{i,5} \le 100\% u^3_{i,5} \end{cases} \tag{36}$$

$$u^3_{i,1} + u^3_{i,2} + u^3_{i,3} = 1 \tag{37}$$

$$u^3_{i,4} + u^3_{i,5} + u^3_{i,6} = 1 \tag{38}$$

where $SOE^3_{i,1}$, $SOE^3_{i,2}$ and $SOE^3_{i,3}$, $SOE^3_{i,4}$, $SOE^3_{i,5}$ and $SOE^3_{i,6}$ are the auxiliary variables to represent the $SOE^3_i$ in 3 piece-wise sections for discharging behavior charging behavior respectively.

In each $\Delta d_i$, the maximum discharged or charged energy of each type of OESD, $\overline{E^k_{i,dch}}$ and $\overline{E^k_{i,ch}}$, should follow the limitation of its maximum discharge and charge power and the elapsed running time. Thus, it can be expressed as shown in (39).

$$\overline{E^k_{i,dch}} = \overline{P^k_{i,dch}} \Delta t_i, \quad \overline{E^k_{i,ch}} = \overline{P^k_{i,ch}} \Delta t_i \tag{39}$$

It is easily observed that that the maximum discharged/charged energy of OESD is determined by a product of two variables, $\overline{P^k_{i,dch}}$ (and $\overline{P^k_{i,ch}}$) and $\Delta t_i$. In this case, the linearization on this product needs to be conducted and the method can be found in [40]. The auxiliary variables $y^k_{i,1}$, $y^k_{i,2}$, $y^k_{i,3}$ and $y^k_{i,4}$ are introduced, as shown in (40) and (41).

$$y^k_{i,1} = \frac{1}{2}(\overline{P^k_{i,dch}} + \Delta t_i), \quad y^k_{i,2} = \frac{1}{2}(\overline{P^k_{i,dch}} - \Delta t_i) \tag{40}$$

$$y^k_{i,3} = \frac{1}{2}(\overline{P^k_{i,ch}} + \Delta t_i), \quad y^k_{i,4} = \frac{1}{2}(\overline{P^k_{i,ch}} - \Delta t_i) \tag{41}$$

In this case, it has the relationships as shown in (42) and (43).

$$\overline{E^k_{i,dch}} = \overline{P^k_{i,dch}} \Delta t_i = (y^k_{i,1})^2 - (y^k_{i,2})^2 \tag{42}$$

$$\overline{E^k_{i,ch}} = \overline{P^k_{i,ch}} \Delta t_i = (y^k_{i,3})^2 - (y^k_{i,4})^2 \tag{43}$$

Here 2 series of piecewise points $Y^{k,dch}_j$ and $Y^{k,ch}_j$ are used to represent $y^k_{i,1}$, $y^k_{i,2}$, $y^k_{i,3}$ and $y^k_{i,4}$. In this case, (42) and (43) can be reformulated into (44) and (45).

$$\overline{E^k_{i,dch}}' = \sum_{j=1}^{J_2} (Y^{k,dch}_j)^2 \alpha^{k,dch}_{i,j} - \sum_{j=1}^{J_2} (Y^{k,dch}_j)^2 \beta^{k,dch}_{i,j} \tag{44}$$

$$\overline{E^k_{i,ch}}' = \sum_{j=1}^{J_3} (Y^{k,ch}_j)^2 \alpha^{k,ch}_{i,j} - \sum_{j=1}^{J_3} (Y^{k,ch}_j)^2 \beta^{k,ch}_{i,j} \tag{45}$$

$\alpha^{k,dch}_{i,j}$, $\beta^{k,dch}_{i,j}$, $\alpha^{k,ch}_{i,j}$ and $\beta^{k,ch}_{i,j}$ are 4 sets of SOS2 variables for each type of OESD in $\Delta d_i$, and $J_2$ and $J_3$ are the number of the corresponding piece-wise points. As a result, they also need to follow the (46) - (49).

$$\sum_{j=1}^{J_2} \alpha^{k,dch}_{i,j} = 1, \quad \sum_{j=1}^{J_2} \beta^{k,dch}_{i,j} = 1 \tag{46}$$

$$\sum_{j=1}^{J_3} \alpha^{k,ch}_{i,j} = 1, \quad \sum_{j=1}^{J_3} \beta^{k,ch}_{i,j} = 1 \tag{47}$$

$$0 \le \alpha^{k,dch}_{i,j} \le 1, \quad 0 \le \beta^{k,dch}_{i,j} \le 1 \tag{48}$$

$$0 \le \alpha^{k,ch}_{i,j} \le 1, \quad 0 \le \beta^{k,ch}_{i,j} \le 1 \tag{49}$$

To ensure that only the adjacent $\alpha^{k,dch}_{i,j}$, $\beta^{k,dch}_{i,j}$, $\alpha^{k,ch}_{i,j}$ and $\beta^{k,ch}_{i,j}$ can be nonzero and their sum being 1, 0-1 variables $\mu^{k,dch_\alpha}_{i,j}$

and $\mu_{i,j}^{k,dch_\beta}$, $\mu_{i,j}^{k,ch_\alpha}$ and $\mu_{i,j}^{k,ch_\beta}$ need to be imposed, as shown in (50) - (53).

$$\alpha_{i,j}^{k,dch} + \alpha_{i,j+1}^{k,dch} - \mu_{i,j}^{k,dch_\alpha} \geq 0, \beta_{i,j}^{k,dch} + \beta_{i,j+1}^{k,dch} - \mu_{i,j}^{k,dch_\beta} \geq 0 \tag{50}$$

$$\alpha_{i,j}^{k,ch} + \alpha_{i,j+1}^{k,ch} - \mu_{i,j}^{k,ch_\alpha} \geq 0, \quad \beta_{i,j}^{k,ch} + \beta_{i,j+1}^{k,ch} - \mu_{i,j}^{k,ch_\beta} \geq 0 \tag{51}$$

$$\sum_{j=1}^{J_2-1} \mu_{i,j}^{k,dch_\alpha} = 1, \quad \sum_{j=1}^{J_2-1} \mu_{i,j}^{k,dch_\beta} = 1 \tag{52}$$

$$\sum_{j=1}^{J_3-1} \mu_{i,j}^{k,ch_\alpha} = 1, \quad \sum_{j=1}^{J_3-1} \mu_{i,j}^{k,ch_\beta} = 1 \tag{53}$$

### *D. Constraints and Objective of the MILP Model*

Mixed integer linear programming (MILP) problem is with an objective function and constraints that are linear with integer variables presented [41]. Different from the linear optimization problems, at least some of the variables in MILP problems are constrained to take on integer values. The general form of a MILP problem is shown in (54).

$$\begin{aligned} \min \quad & c_0 + \sum_{i=1}^{n} c_i x_i \\ \text{s.t.} \quad & \sum_{i=1}^{n} A_j^e x_i = b_j^e, && \forall j = 1, ..., l_e \\ & \sum_{i=1}^{n} A_j^{ine} x_i \leq b_j^{ine}, && \forall j = 1, ..., l_{ine} \\ & x_i \in \mathbb{Z}, && \text{for some} \quad i = 1, ..., n \\ & x_i \in \mathbb{R}, && \text{for the remaining} \quad i = 1, ..., n, \end{aligned} \tag{54}$$

where $x_1, ..., x_n$ are the decision variables to be optimized. $l_e$ and $l_{ine}$ are the numbers of equality and inequality constraints. Thus, $l_e$+$l_{ine}$ is the total number of constraints. The coefficients, $A_j^e$, $A_j^{ine}$, $l_e$ and $l_{ine}$, the terms on the right-hand sides of the constraints, $b_j^e$ and $b_j^{ine}$ and the coefficients, $c_o, ..., c_n$, in the objective function are all constants. Since the optimal train driving strategy with OESD for electrified railway systems is formulated into a MILP problem, the constraints and objective of the model need to be adjusted accordingly with consideration of this specific problem.

First, the initial speed $v_1$, terminal speed $v_{N+1}$ and the speed limit need to be preset as in (55).

$$v_1^2 = V_{ini}^2, \quad v_{N+1}^2 = V_{ter}^2, \quad v_i^2 = \overline{V_i}^2 \tag{55}$$

To ensure the riding comfort of the passengers and the operational limit of the train vehicle, the acceleration/deceleration should be limited by the maximum allowed value, as shown in (56).

$$-\underline{a} \leq a_i \leq \overline{a} \tag{56}$$

According to the law of conservation of the energy, the conversion of the energy can be expressed in (57).

$$E_{i,m} + E_{i,r} - E_{i,v} - E_{i,f} - E_{i,p} \geq 0 \tag{57}$$

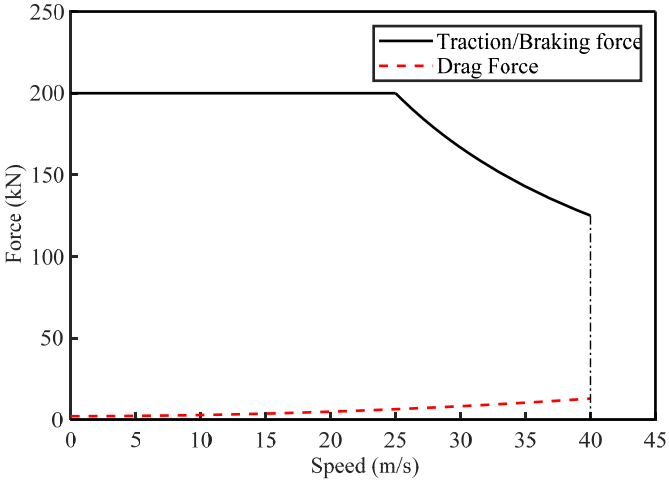


Fig. 6. The traction/braking characteristics and drag force of the train vehicle of the case studies, where the maximum traction/braking force and power are 200 kN and 5000 kW. The Davis coefficient A, B and C can be calibrated to be 2.0895 kN, 0.0098 kN $\cdot$ s/m and 0.0065 kN $\cdot$ s$^2$/m$^2$. Noted that each of these values can be adjusted according to the field data of the actual traction systems.

In addition, the power limit of the motor and OESD should be added as the constraints respectively. For the motor, (58) - (59) are used to ensure the force and power that the motor supplies in both traction mode and braking mode does not exceed the maximum allowed value.

$$E_{i,s}\eta_s + E_{i,dch}^k \eta_k \leq \overline{E_{i,t}^F}, \quad E_{i,s}\eta_s + E_{i,dch}^k \eta_k \leq \overline{E_{i,t}^P} \tag{58}$$

$$\frac{E_{i,ch}^k}{\eta_k} \leq \overline{E_{i,b}^F}, \quad \frac{E_{i,ch}^k}{\eta_k} \leq \overline{E_{i,b}^P} \tag{59}$$

For $k$-type OESD, the discharged and charged energy cannot exceed the maximum value determined by the maximum charge and discharge power, as expressed in (60).

$$E_{i,dch}^k \leq \overline{E_{i,dch}^k}', \quad E_{i,ch}^k \leq \overline{E_{i,ch}^k}' \tag{60}$$

To guarantee the punctuality and operational requirement, the constraint of total journey time $T$ should be added, as shown in (61).

$$\sum_{i=1}^{N} \Delta t_i = T \tag{61}$$

The stored energy in the OESD need to be higher than 0 and lower than 100%, thus constraint (62) needs to be added into the model.

$$0 \leq SOE_i^k \leq 100\% \tag{62}$$

In addition, the initial SOE of the OESD when the train departs from the first station can be set to be $SOE_{ini}$ thus we have constraint (63).

$$SOE_1^k = SOE_{ini} \tag{63}$$

The objective functions of the model for all three OESDs are the same but with different constraints. The objective function is defined to minimize the net energy consumption

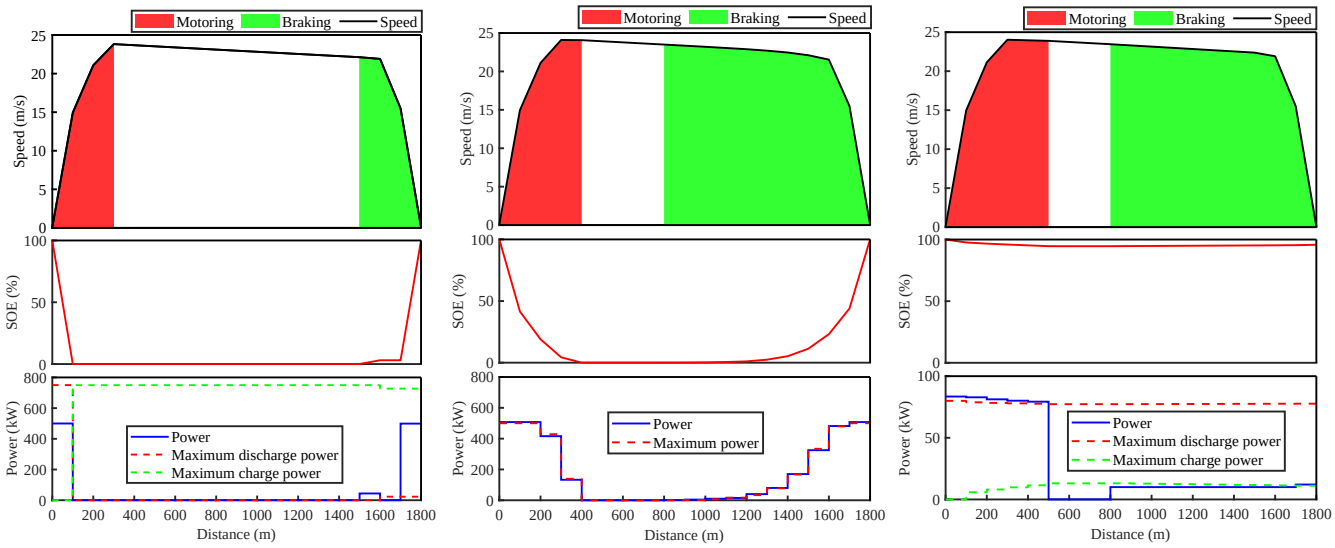


Fig. 7. Scenario 1: The optimal train speed, OESD SOE and power profiles for the train with (a) supercapacitor, (b) flywheel and (c) Li-ion battery on a 1800-meter-long flat track without speed limits. Different motoring and braking distribution resulted from different OESD, where 300-meter-long motoring and braking distance for supercapacitor, 400-meter-long motoring distance and 900-meter-long braking distance for flywheel and 500-meter-long motoring distance and 900-meter-long braking distance for Li-ion battery. Also, the OESD power is limited by their own dynamic power limits with a slight violation due to the modeling precision, which is to be explained in Section IV-D.

which is the total traction energy consumption deducted by the total regenerative energy received by OESDs. Here the models for finding the optimal driving strategy for the train with supercapacitor, flywheel and Li-ion battery are given in (64).

$$\begin{aligned} \min \quad & \sum_{i=1}^{N}(E_{i,s} + E_{i,dch}^{k} - E_{i,ch}^{k}), \\ \text{s.t.} \quad & (21)-(63), \quad for \quad k = 1, 2, 3. \end{aligned} \tag{64}$$

The proposed MILP model can be solved by a commercial solver e.g. CPLEX®, Lingo® or Gurobi® etc. to efficiently determine the optimal driving strategy of the train with OESDs. The optimal speed profile can be chosen by the model itself when inputting the relevant parameters of the railway system and OESD used as the constraints. In this case, the speed profile, including motoring/coasting/braking behaviors, can be chosen freely as long as the net energy consumption is minimized for the whole journey.

## IV. Case Studies and Results Discussion

In this section, the case studies for various scenarios are conducted by using the proposed model. There are four scenarios in the case studies and listed as following:

- Train operation with OESDs without the varied route conditions (runs on flat track and no speed limits).
- Train operation with OESDs with the varied route conditions (runs on sloping track and varied speed limits).
- Train operation with OESDs on partial discontinuously electrified railway.
- Train operation with OESDs on catenary-free railways.

The results of these case studies show the adaptive eco-driving strategy of the train with different types of OESD adopted in the research, as well as their respective influence on train operations. In the case studies, mainly the generic urban railway systems, e.g. metro systems, tram systems with relatively short distance and short journey time between adjacent stations, are used to test our model. However, the journey time or track length can also be prolonged based on (61) which controls the journey time according to the real operational requirement, such as the metro ad tram systems with short-time operation in the paper or even the high-speed railways with long time operation.

The train traction/braking characteristics and the drag force used in the case studies are shown in Figure 6. The mass of the train $M_t$ in the case studies is 176 t without the OESD and the maximum acceleration $\overline{a}$ and deceleration $\underline{a}$ are both set to be 1.2 $\mathrm{m/s^2}$. The track length $D$ is equally divided to be 100 m for all of the scenarios. The average energy efficiency $\eta_s$ and $\eta_k$ can be set based on literature from long-term viewpoint. Specifically, the energy transmission efficiency from grid to the motor is set as 90% due to a 10% average energy loss and the energy conversion efficiency of electric motor is set as 90% for most typical engineering applications [2]. Therefore, the approximated value for $\eta_s$ is 81% = 90% $\times$ 90% in this study. On the other hand, energy can be directly transmitted between the motor and OESD with a negligible transmission loss [37], thus, the value for $\eta_k$ is set as 90% considering only the discharge/charge efficiency resulted from the OESD's own resistance. Both values can be modified according to the field

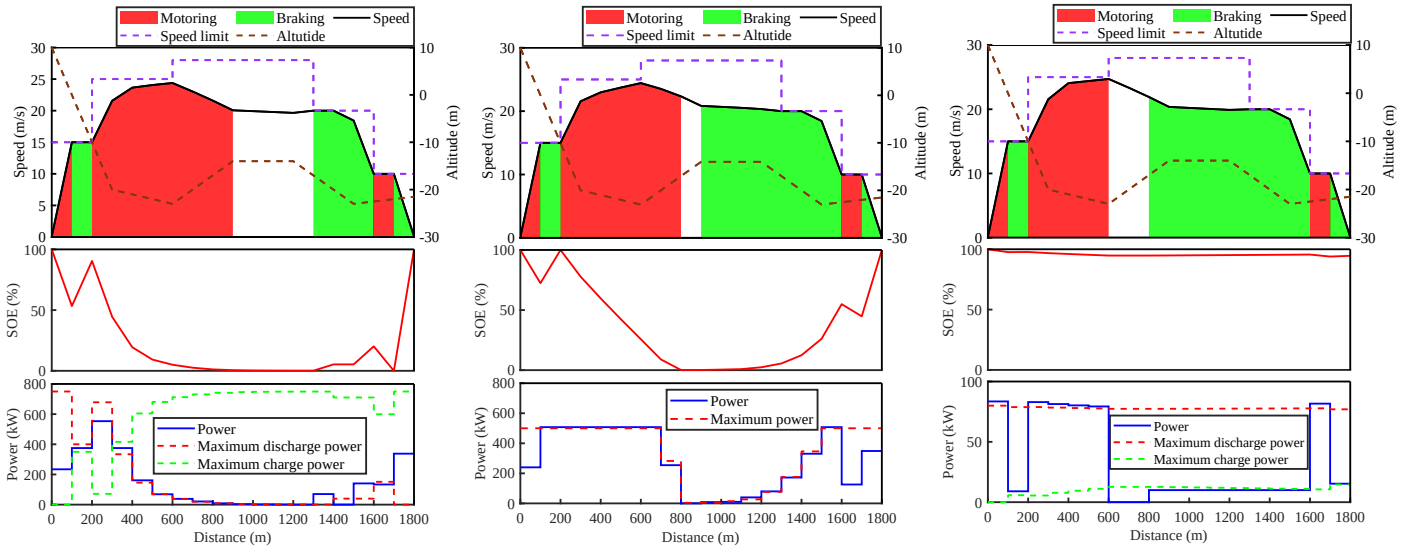


Fig. 8. Scenario 2: The optimal train speed, OESD SOE and power profiles for the train with (a) supercapacitor, (b) flywheel and (c) Li-ion battery on a 1800-meter-long sloping track with speed limits. Different motoring and braking distribution resulted from different OESD, both of the optimal speed and OESD discharge/charge power are limited by the speed limits and dynamic power limits respectively during the journey.

data. Note that the case studies are conducted by using Matlab R2020a® and Gurobi® 9.0.1 solver on a PC with Intel Core® i5-5200U processor (2.20 GHz) and 8.00 GB RAM.

### A. *Without/with Varied Route Conditions*

Since the case study is for the train running between two adjacent stations, the track length is set to be 1800 m and the initial speed $v_1$ and the terminal speed $v_{N+1}$ of the train should be 0. Each kind of OESD is assumed to be fully charged, namely $SOE_{ini}$= 100%, before the departure of the train.

Scenario 1 of the case study is to explore the optimal eco-driving strategy for train with different types of OESD on the flat track without speed limits, and the running time $T$ is limited at 100 s. The optimal speed profiles, train operation mode, OESD power and SOE profiles are illustrated in Figure 7, and it is evident that the optimal eco-driving strategies of the train with different types of OESD are significantly different. For the train with supercapacitor, the SOE and power profiles show that its SOE and power limit drop/soar fast during the journey resulted from its highest maximum power and lowest capacity among the three types of OESD. This in turns results in the shortest motoring distance/braking distance and longest coasting distance. For the train with flywheel, the OESD always works at its power limits due to its larger capacity of and lower maximum power, leading to the longer discharge/charge process and longer motoring/braking distance than supercapacitor. As for the train with Li-ion battery, due to its largest capacity and lowest maximum power, the discharge/charge process of it is the most frequent among the three, leading to the constant motoring/braking to make the OESD release and recover as mush energy as possible.

Scenario 2 is to see the flexibility of the proposed method, where the varied route conditions e.g. gradient change and speed limits are introduced to make the case studies more practical, and the running time $T$ is prolonged to be 120 s here since the maximum train speed is constrained by speed limits. The results are shown in Figure 8, which shows that due to the introduction of the complex route conditions the train speed, SOE and power profiles see significant difference compared to scenario 1. Different optimal eco-driving strategies for the train with different types of OESD can be found to meet the real operational requirements, where the discharge/charge process for three types of OESD still follow the corresponding dynamic power limit. Discharge/charge processes are more frequent than scenario 1 resulted from the introduced route conditions. The train switches the motoring and braking back and forth to finish the journey, where the SOE and power profiles for supoercapacitor and flywheel are more fluctuated than the scenario 1 while SOE of Li-ion battery still changes mildly.

### B. *Discontinuously Electrified and Catenary-free Railways*

Though railway electrification prevails in some region and country in recent years, in some special locations, e.g. tunnel or bridges, installing the catenary or other power supply systems might be economically or technically impractical. On the other hand, some of the railway systems are too old to be fully electrified, e.g. the TransPennine route between Leeds and Manchester built in Victorian times [42]. In addition, the future projects should ensure that all options for traction power supplies are considered, including distribution and energy storage options on the discontinuous electrification, where the operating and maintenance costs and the resilience

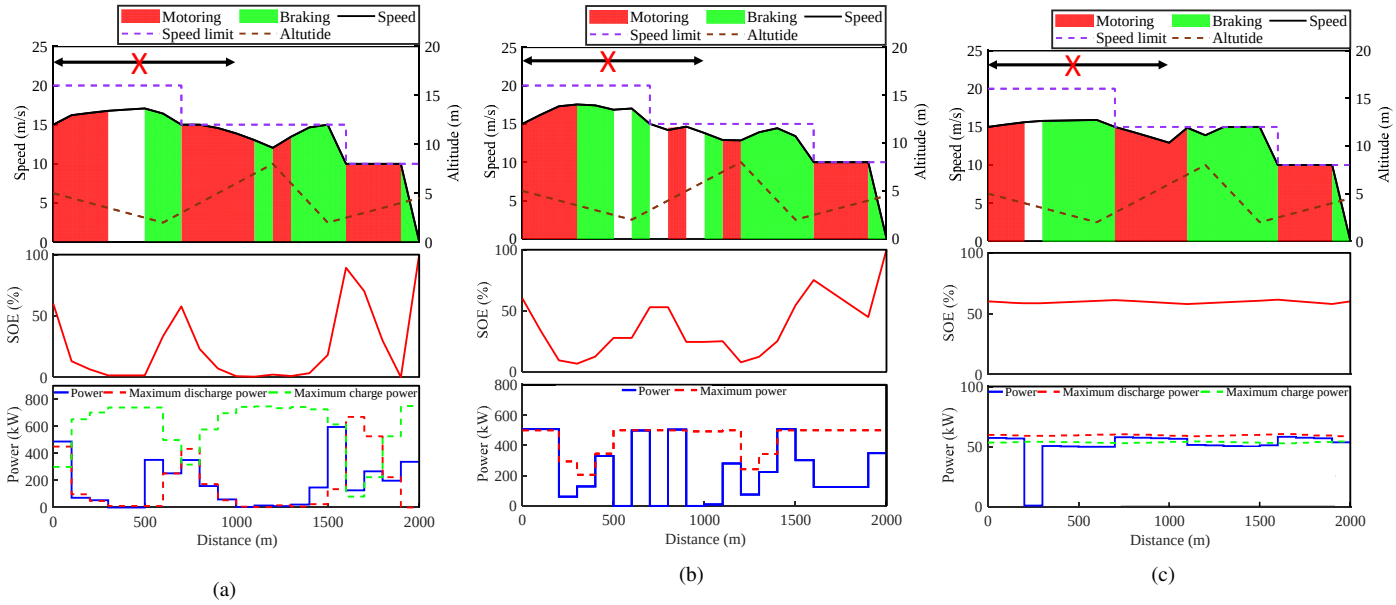


Fig. 9. Scenario 3: The optimal train speed, OESDs' SOE and OESD power profiles for (a) supercapacitor, (b) flywheel and (c) Li-ion battery with non-electrified sections (The double arrow with "X" represents the non-electrified section). During the running in the non-electrified section, the train with different OESD conducts more motoring than braking, e.g. 600-meter-long motoring VS 200-meter-long braking for supercapacitor, 400-meter-long motoring VS 200-meter-long braking for flywheel and 500-meter-long motoring VS 400-meter-long braking for Li-ion battery.

of the alternatives should also be considered [43]. When the train is equipped with OESD, if well designed, the train can always secure adequate energy supply and operate on railway sections without temporary or permanent electricity supply from substations. In this section, the potential of each types of OESD applied in discontinuously-electrified and catenary-free railways is investigated. In Scenario 3, the train is running on a 2000-m track with a non-zero initial speed and a 1000 m non-electrified section at the beginning. The total running time $T$ is assumed to be 160 s and the new speed limits and gradients information are also introduced. In scenario 3, the initial speed $v_1$ and the initial SOE of OESD $SOE_1^k$ when entering the non-electrified section is assumed to be 15 m/s and 60% respectively.

Since the train running in the first 1000 meters cannot be powered by the substation, thus, the $1^{st}$ to $10^{th}$ $E_{i,s}$ need to be set as 0. The results of scenario 3 are shown in Figure 9, it can be observed that the train can safely passes the non-electrified section under the support of OESD, and the speed profiles with different types of OESD are noticeably different. The motoring and braking process together with the discharge/charge process of OESD occur repeatedly along with the journey. In addition, it can also be noted that the SOE change of Li-ion battery is still much more mild than that of supercapacitor and flywheel.

On the other hand, trains running on the catenary-free railway is also common in city trams or light rail systems. The proposed method can be used to evaluate the feasibility of each type of OESD in catenary-free railway lines using time-saving driving strategy. To achieve this, scenario with the track length being 2500 m with speed limits and gradient information is given. The objective function of the model needs to be revised to be (65), with the constraint of the total running time (61) relaxed and all of the $E_{i,s}$ set to be 0.

$$\min \quad \sum_{i=1}^{N} \Delta t_i \tag{65}$$

By changing the objective function to minimize the total running time, the time-saving potential of the train with each type of OESD can be obtained, and the optimal speed profiles, SOE profile, OESD power profile and corresponding time-distance paths are shown in Figure 10. It can be noted from the results that the train with flywheel can run faster than the other two because it makes the shortest total running time. Though with the highest maximum power, the small capacity of the supercapacitor undermines its time-saving driving strategy very much, resulting in the longest running time among the three. On contrary, due to the largest capacity of the Li-ion battery, the train with it can have constant but lowest power supply. This ensures that the train with it can constantly motor to accelerate for reducing the journey time, just as shown in Figure 10(c). Also, from the change of the SOE and OESD power profile, though each of the three sees significant difference, the similar trend is to power the train as much as possible to raise the speed rather than recovering the regenerative energy.

### C. Energy-saving Potential Comparison and Discussion

For a comprehensive evaluation and comparison, the net energy consumption, energy-saving rate and the energy-saving rate per k$ for all scenarios are given in Table IV. Noted that the unit in kWh is used to reduce the digit numbers when using unit kJ of the variables. From the result of scenario 1, it can

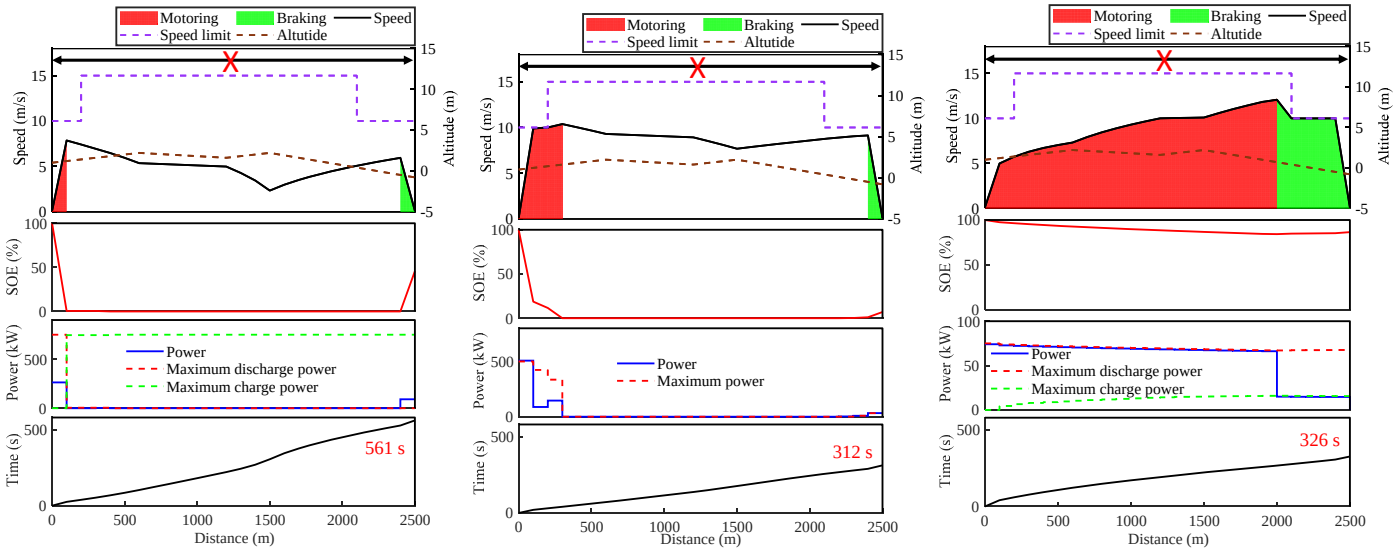


Fig. 10. Scenario 4: The optimal train speed profile, SOE profile and OESD power profile and corresponding time-distance path for (a) supercapacitor, (b) flywheel and (c) Li-ion battery on the catenary-free railway section (The double arrow with "X" represents the non-electrified section). Different shortest journey time resulted from different OESD are shown, where the flywheel can bring the fastest arrival, Li-ion battery ranks the second and supercapacitor ranks the last.

TABLE IV
RESULTS OF THE CASE STUDIES

| OESD type | Energy supplied by OESD (kWh) | Energy recovered by OESD (kWh) | Energy dissipated by resistor (kWh) | Energy from catenary (kWh) | Net energy consumption (kWh) | Energy-saving rate (%) | Energy-saving rate per k$ (%/k$) |
|---|---|---|---|---|---|---|---|
| Scenario 1: without varying route conditions (1800-meter-long track and 100-second journey time) | | | | | | | |
| Supercapacitor | 1.87 | 1.87 | 9.60 | 15.76 | 15.76 | 13.55 | 0.09 |
| Flywheel | 3.50 | 3.50 | 8.18 | 14.46 | 14.46 | 22.32 | 0.15 |
| Li-ion battery | 0.16 | 0.75 | 10.63 | 18.64 | 18.05 | 0.99 | 0.01 |
| Scenario 2: with varying route conditions (1800-meter-long track and 120-second journey time) | | | | | | | |
| Supercapacitor | 2.94 | 2.94 | 14.24 | 2.49 | 2.49 | 59.24 | 0.39 |
| Flywheel | 4.82 | 4.82 | 12.93 | 1.42 | 1.42 | 76.76 | 0.51 |
| Li-ion battery | 0.22 | 0.97 | 15.95 | 6.58 | 5.83 | 4.58 | 0.03 |
| Scenario 3: partially electrified railway (2000-meter-long track and 160-second journey time) | | | | | | | |
| Supercapacitor | 3.86 | 4.61 | 2.17 | 0 | -0.75 | 115 | 0.77 |
| Flywheel | 4.54 | 5.94 | 1.29 | 0 | -1.40 | 129 | 0.86 |
| Li-ion battery | 1.15 | 1.16 | 5.89 | 2.91 | 2.90 | 39.71 | 0.26 |
| Scenario 4: catenary-free railway (2500-meter-long track) | | | | | | | |
| Supercapacitor | 1.87 | 0.86 | 0 | 0 | 1.01 | / | / |
| Flywheel | 3.50 | 0.24 | 1.89 | 0 | 3.25 | / | / |
| Li-ion battery | 5.35 | 0.96 | 2.73 | 0 | 4.38 | / | / |

be seen that except of Li-ion battery, both supercapacitor and flywheel have ran out of their stored energy since their supplied energy equal to their capacity. For scenario 2 and scenario 3, due to the more frequent discharge/charge process during the journey resulted by the more complex route conditions, the supplied energy and recovered energy by supercapacitor and flywheel are higher than their capacity. The net energy consumption of scenario 3 for both supercapacitor and flywheel is negative. This is resulted from the non-zero initial speed of the journey, where the energy consumption of the previous running is not counted in the results, and also due to the more energy recovered than energy supported of both type of OESD in this journey.

It can be seen that from scenario 1 to scenario 3, the train with flywheel are always with minimum net energy consumption on the same route when compared to the train with the supercapacitor and Li-ion battery. Flywheel can also supply and recover the most energy during the journey, resulting in the least dissipated energy by resistor. On the other hand, the Li-ion battery brings the least energy-saving effect, with the highest net energy consumption from scenario 1 to scenario 3. Li-ion battery can only supply and recover few energy due to its limited power capability, resulting in the most dissipated energy among the three types of OESD.

For Scenario 4, it should be noted that the objective of it is not on energy saving but on feasibility analysis. With the catenary-free railways, it is observed that Li-ion battery supplies the most energy and recovers the most energy during

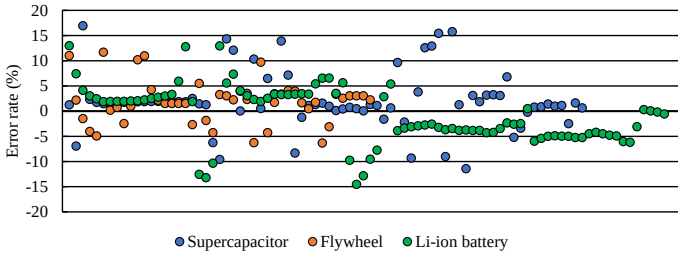


Fig. 11. The error rate for dynamic power limits approximation of each types of OESD from the case studies.

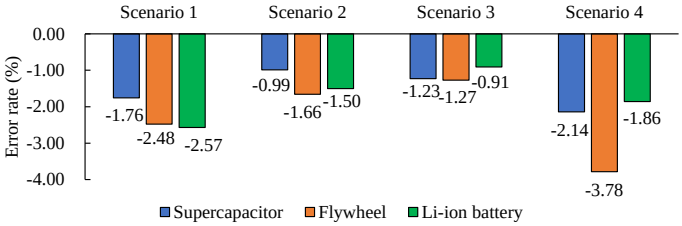


Fig. 12. The error rate for running time modeling for each OESD in various case studies.

the journey. This is resulted from its largest capacity which enables it to have continuous traction and braking to save the running time of the journey. In contrary, due to the smallest capacity of the supercapacitor, though it can supply the highest power in short time, the train still has limited traction ability which undermines the time-saving effect.

In summary, based on the optimization results of the 4 scenarios shown above, the technical advantages of these three types of OESD can be analyzed on the average term. From the results tabulated in Table IV, it can be seen that the flywheel can bring the least catenary energy consumption and net energy consumption with the highest energy-saving rate, ranging from 22.32% to 129%, and also the most cost-effective for its highest energy-saving rate per k$. Though the supercapacitor and the Li-ion battery bring less energy-saving rate than the flywheel, under the same capital cost the supercapacitor can provide the highest power output in a short time while the Li-ion battery is with the largest capacity for the long-term operation. It also implies that the proper combination of them will make the most of each type of OESD, which might help reduce more energy consumption.

### *D. Error Analysis of the Proposed Method*

In this section, the error analysis of the proposed method is elaborated by focusing on power limits $\overline{P^k_{idch}}$ and $\overline{P^k_{ich}}$ and the running time $T$ based on the results of the case studies.

In section III, linear approximation of the train movement and the dynamic power characteristics of three types of OESD are conducted, which leads to the difference between the approximated value and actual value. This can be observed in the results that there are slight discrepancies between the OESD power profile and the corresponding power limits. For scenario 1, in Figure 7(c), it can be seen that the discharge power of Li-ion battery slightly exceeds its power limits. For scenario 2, it can be observed in Figure 8(a) and Figure 8(c) that the discharge and charge power for both supercapacitor and Li-ion battery are slightly higher than their respective limits in some $\Delta d_i$. Also, the discharge power of supercapacitor in scenario 3, as shown in Figure 9(a), sometimes goes beyond the power limits a bit during the journey.

The dynamic power limits with respect to the current SOE of OESD for different types of OESD are approximated by using piece-wise linearization and SOS2 method in the modeling process. As a result, the error analysis of it is needed to see the performance of the proposed approach. The error rate of the discharge/charge power limit, $e^{dch}_{i,P}$ and $e^{ch}_{i,P}$, can be obtained by using (66).

$$e^{dch}_{i,P} = \frac{\frac{\overline{E^k_{i,dch}}'}{\Delta t_i} - \overline{P^k_{i,dch}}}{\overline{P^k_{i,dch}}} \times 100\%, e^{ch}_{i,P} = \frac{\frac{\overline{E^k_{i,ch}}'}{\Delta t_i} - \overline{P^k_{i,ch}}}{\overline{P^k_{i,ch}}} \times 100\% \tag{66}$$

Note that the error data when $\overline{P^k_{i,dch}}$ or $\overline{P^k_{i,ch}}$ equals to 0 are eliminated in the results due to the infeasible calculation. The results of the error rate is plotted in Figure 11. From the figure, it can be seen that the most of the points are located between $\pm 5\%$ in error rate data for all of the $\Delta d_i$ of the case studies. Additionally, the average error rate for supercapacitor, flywheel and Li-ion battery is 2.04%, 1.84% and -0.71% respectively, showing that the proposed method preforms satisfactorily on modeling the dynamic power limits of each types of OESD.

On the other hand, the relationships among the speed-related variables are linearized by using SOS2, and the approximated values $\frac{1}{v'_{i,ave}}$ but not the real reciprocal of average speed of each $\Delta d_i$ are used in calculating the running time $T$, which influences the accuracy of it. Since punctuality is important in real operation, the accuracy of it in the proposed model is also essential, which indicates that the error analysis of the running time is necessary. Here the error rate of the running time $T$ is denoted as $e_T$, and it can be calculated by dividing the difference of the approximated values and real values by the real values, as shown in (67).

$$e_T = \frac{T - (\sum_{i=1}^{N} \frac{\Delta d_i}{\sqrt{v_i^2 + \sqrt{v_{i+1}^2}}})}{\sum_{i=1}^{N} \frac{\Delta d_i}{\sqrt{v_i^2 + \sqrt{v_{i+1}^2}}}} \times 100\% \tag{67}$$

Based on the obtained optimal speed profiles, the $e_T$ for 4 scenarios of these three types of OESD can be calculated, the results of which are illustrated in Figure 12. It can be observed that the error rates of the running time for 4 scenarios of three types of OESD are all small, the range of which are only between -0.91% and -3.78%, while the average error rate being -1.8%. This error rate is relatively small when comparing with the error rate 5% in [44] and 2% in [45] dealing with the train speed optimization using mathematical programming. This confirms the acceptable modeling accuracy of our method on controlling the running time of the journey.

## V. Conclusion

This paper has investigated the optimal driving strategy of the electric train equipped with three popular types of OESD: supercapacitors, flywheels and Li-ion batteries, to minimize the net energy consumption by taking into account their corresponding dynamic discharge/charge characteristics. The dynamic power limits of different types of OESD of the fixed investment cost together with the train operation are formulated as a mixed integer linear programming (MILP) problem. The case studies are conducted by using the proposed method and investigate the train operation on fully electrified railways, partially electrified railways and catenary-free railways. Based on the results, insightful comparisons of the speed profiles, SOE and power profiles of OESDs and energy-saving effect for the train with different type of OESD are given. It can be seen from the results that flywheel offers the best performance on saving the energy consumption with the highest energy-saving rate ranging from 0.15 %/k$ to 0.86 %k$ under various scenarios. Supercapacitor ranks the second and can save the energy consumption from 0.09 %/k$ to 0.77 %/k$. Li-ion battery sees the poorest performance since it can only bring a energy-saving rate from 0.01 %/k$ to 0.26 %/k$ for all of the scenarios. In addition, from the error rate analysis it can be told that the proposed method can solve the problem with acceptable modeling accuracy, which shows the effectiveness and practicality of the approach.

Since the study mainly focuses on the short-term train operation optimization problem, in the future, other long-term time-variant factors, such as the depth of discharge and cycling lifetime of the OESD can also be integrated into the proposed framework to conduct a long-term evaluation, which might lead to more practical optimal results. In addition, the hybrid energy storage system, e.g. batteries with supercapacitors, can also be integrated to make the most of each type of OESD to save energy consumption based on the findings of this paper.

## References


[1] UIC-IEA, "Railway handbook 2017," 2017.

[2] A. González-Gil, R. Palacin, P. Batty, and J. Powell, "A systems approach to reduce urban rail energy consumption," *Energy Conversion and Management*, vol. 80, pp. 509–524, 2014.

[3] N. Ghaviha, J. Campillo, M. Bohlin, and E. Dahlquist, "Review of application of energy storage devices in railway transportation," *Energy Procedia*, vol. 105, pp. 4561 – 4568, 2017, 8th International Conference on Applied Energy, ICAE2016, 8-11 October 2016, Beijing, China.

[4] A. S. Abdelrahman, Y. Attia, K. Woronowicz, and M. Z. Youssef, "Hybrid fuel cell/battery rail car: A feasibility study," *IEEE Transactions on Transportation Electrification*, vol. 2, no. 4, pp. 493–503, 2016.

[5] X. Liu and K. Li, "Energy storage devices in electrified railway systems: A review," *Transportation Safety and Environment*, no. 3, p. 3, 2020.

[6] R. Barrero, J. Van Mierlo, and X. Tackoen, "Energy savings in public transport," *IEEE vehicular technology magazine*, vol. 3, no. 3, pp. 26–36, 2008.

[7] R. Barrero, X. Tackoen, and J. Van Mierlo, "Stationary or onboard energy storage systems for energy consumption reduction in a metro network," *Proceedings of the Institution of Mechanical Engineers, Part F: Journal of Rail and Rapid Transit*, vol. 224, no. 3, pp. 207–225, 2010.

[8] M. Domínguez, A. Cucala, A. Fernández, R. Pecharromán, and J. Blanquer, "Energy efficiency on train control: design of metro ato driving and impact of energy accumulation devices," in *9th World Congress on Railway Research – WCRR 2011*, vol. 2011, 2011.

[9] M. Chymera, A. Renfrew, and M. Barnes, "Analyzing the potential of energy storage on electrified transit systems," in *8th World congress of railway research–WCRR*, vol. 2008, 2008.

[10] B. Destraz, P. Barrade, A. Rufer, and M. Klohr, "Study and simulation of the energy balance of an urban transportation network," in *2007 European conference on power electronics and applications*. IEEE, 2007, pp. 1–10.

[11] J.-P. Moskowitz and J.-L. Cohuau, "Steem: Alstom and ratp experience of supercapacitors in tramway operation," in *2010 IEEE Vehicle Power and Propulsion Conference*. IEEE, 2010, pp. 1–5.

[12] M. Spiryagin, P. Wolfs, F. Szanto, Y. Q. Sun, C. Cole, and D. Nielsen, "Application of flywheel energy storage for heavy haul locomotives," *Applied energy*, vol. 157, pp. 607–618, 2015.

[13] A. Rupp, H. Baier, P. Mertiny, and M. Secanell, "Analysis of a flywheel energy storage system for light rail transit," *Energy*, vol. 107, pp. 625–638, 2016.

[14] H. Hayashiya, T. Suzuki, K. Kawahara, and T. Yamanoi, "Comparative study of investment and efficiency to reduce energy consumption in traction power supply: A present situation of regenerative energy utilization by energy storage system," in *2014 16th International Power Electronics and Motion Control Conference and Exposition*. IEEE, 2014, pp. 685–690.

[15] M. Ogasa, "Application of energy storage technologies for electric railway vehicles—examples with hybrid electric railway vehicles," *IEEJ Transactions on Electrical and Electronic Engineering*, vol. 5, no. 3, pp. 304–311, 2010.

[16] A. Rufer, "Energy storage for railway systems, energy recovery and vehicle autonomy in europe," in *The 2010 International Power Electronics Conference-ECCE ASIA-*. IEEE, 2010, pp. 3124–3127.

[17] L. Cheng, P. Acuna, S. Wei, J. Fletcher, W. Wang, and J. Jiang, "Fast-swap charging: An improved operation mode for catenary-free light rail networks," *IEEE Transactions on Vehicular Technology*, vol. 67, no. 4, pp. 2912–2920, 2018.

[18] Z. Zhong, Z. Yang, X. Fang, F. Lin, and Z. Tian, "Hierarchical optimization of an on-board supercapacitor energy storage system considering train electric braking characteristics and system loss," *IEEE Transactions on Vehicular Technology*, vol. 69, no. 3, pp. 2576–2587, 2020.

[19] L. P. Di Noia, F. Genduso, R. Miceli, and R. Rizzo, "Optimal integration of hybrid supercapacitor and ipt system for a free-catenary tramway," *IEEE Transactions on Industry Applications*, vol. 55, no. 1, pp. 794–801, 2019.

[20] C. Wu, S. Lu, F. Xue, L. Jiang, and M. Chen, "Optimal sizing of onboard energy storage devices for electrified railway systems," *IEEE Transactions on Transportation Electrification*, vol. 6, no. 3, pp. 1301–1311, 2020.

[21] J. Chen, H. Hu, Y. Ge, K. Wang, and Z. He, "An energy storage system for recycling regenerative braking energy in high-speed railway," *IEEE Transactions on Power Delivery*, vol. PP, no. 99, pp. 1–1, 2020.

[22] M. Miyatake and K. Matsuda, "Energy saving speed and charge/discharge control of a railway vehicle with on-board energy storage by means of an optimization model," *IEEJ Transactions on Electrical and Electronic Engineering*, vol. 4, no. 6, pp. 771–778, 2009.

[23] M. Miyatake and H. Ko, "Optimization of train speed profile for minimum energy consumption," *IEEJ Transactions on Electrical and Electronic Engineering*, vol. 5, no. 3, pp. 263–269, 2010.

[24] Y. Huang, L. Yang, T. Tang, Z. Gao, F. Cao, and K. Li, "Train speed profile optimization with on-board energy storage devices: A dynamic programming based approach," *Computers  Industrial Engineering*, vol. 126, pp. 149 – 164, 2018.

[25] C. Wu, W. Zhang, S. Lu, Z. Tan, F. Xue, and J. Yang, "Train speed trajectory optimization with on-board energy storage device," *IEEE Transactions on Intelligent Transportation Systems*, vol. 20, no. 11, pp. 4092–4102, 2019.

[26] C. Wu, S. Lu, F. Xue, L. Jiang, and J. Yang, "Optimization of speed profile and energy interaction at stations for a train vehicle with on-board energy storage device," in *2018 IEEE Intelligent Vehicles Symposium (IV)*, June 2018, pp. 1–6.

[27] N. Ghaviha, M. Bohlin, C. Holmberg, and E. Dahlquist, "Speed profile optimization of catenary-free electric trains with lithium-ion batteries," *Journal of Modern Transportation*, Jan 2019.

[28] Z. Xiao, X. Feng, Q. Wang, and P. Sun, "Eco-driving control for hybrid electric trams on a signalised route," *IET Intelligent Transport Systems*, 2019.

[29] F. Yang, L. Lu, Y. Yang, and Y. He, "Characterization, analysis and modeling of an ultracapacitor," *World Electric Vehicle Journal*, vol. 4, no. 2, pp. 358–369, 2010.

[30] D. Yan, L. Lu, F. Jiang, and M. Ouyang, "Comparing the performances of different energy storage cells for hybrid electric vehicle," in *EVS28 International Electric Vehicle Symposium and Exhibition*, 2015.

[31] N. Erd, X. Li, and A. Binder, "Power flow simulation of flywheel energy storage systems for tramways," *Renewable Energy and Power Quality Journal*, vol. 1, no. 15, pp. 149–153, 2017.

[32] X. Li, N. Erd, and A. Binder, "Design and calculation of a 130 kw high-speed permanent magnet synchronous machine in flywheel energy storage systems for urban railway application," in *2017 6th International Conference on Clean Electrical Power (ICCEP)*. IEEE, 2017, pp. 452–459.

[33] R. F. Nelson, "Power requirements for batteries in hybrid electric vehicles," *Journal of power sources*, vol. 91, no. 1, pp. 2–26, 2000.

[34] Y. Cao, S. Tang, C. Li, P. Zhang, Y. Tan, Z. Zhang, and J. Li, "An optimized ev charging model considering tou price and soc curve," *IEEE Transactions on Smart Grid*, vol. 3, no. 1, pp. 388–393, 2011.

[35] C. Z. El-Bayeh, I. Mougharbel, M. Saad, A. Chandra, D. Asber, and S. Lefebvre, "Impact of considering variable battery power profile of electric vehicles on the distribution network," in *2018 4th International Conference on Renewable Energies for Developing Countries (REDEC)*. IEEE, 2018, pp. 1–8.

[36] M. Ceraolo and G. Lutzemberger, "Stationary and on-board storage systems to enhance energy and cost efficiency of tramways," *Journal of Power Sources*, vol. 264, pp. 128 – 139, 2014.

[37] A. González-Gil, R. Palacin, and P. Batty, "Sustainable urban rail systems: Strategies and technologies for optimal management of regenerative braking energy," *Energy conversion and management*, vol. 75, pp. 374–388, 2013.

[38] M. Aneke and M. Wang, "Energy storage technologies and real life applications – a state of the art review," *Applied Energy*, vol. 179, pp. 350 – 377, 2016.

[39] S. Koohi-Fayegh and M. Rosen, "A review of energy storage types, applications and recent developments," *Journal of Energy Storage*, vol. 27, p. 101047, 2020.

[40] J. Bisschop, "Linear programming tricks," *AIMMS-Optimization Modeling*, pp. 63–75, 2006.

[41] R. Sioshansi and A. J. Conejo, *Mixed-Integer Linear Optimization*. Cham: Springer International Publishing, 2017, pp. 123–196.

[42] J. Silmon, "Investigating discontinuous electrification and energy storage on the northern trans-pennine route," *IET Conference Proceedings*, pp. 13–13(1), January 2010.

[43] RIA (Railway Industry Association), "RIA electrification cost challenge," 2019.

[44] Y. Wang, B. De Schutter, B. Ning, N. Groot, and T. J. J. van den Boom, "Optimal trajectory planning for trains using mixed integer linear programming," in *2011 14th International IEEE Conference on Intelligent Transportation Systems (ITSC)*, vol. 19. IEEE, oct 2011, pp. 1598–1604.

[45] Y. Wang, B. De Schutter, T. J. J. van den Boom, and B. Ning, "Optimal trajectory planning for trains – A pseudospectral method and a mixed integer linear programming approach," *Transportation Research Part C: Emerging Technologies*, vol. 29, pp. 97–114, 2013.


**Chaoxian Wu** was born in 1992 in Beihai, Guangxi, China. He received the BEng in Traffic Engineering from Tongji University, Shanghai, China. He was awarded his Intercollegiate MSc degree in Transport & Sustainable Development from Imperial College London, UK and University College London, UK. He is now pursuing the PhD of Electrical Engineering and Electronics from University of Liverpool, UK and also a Visiting Student with the South China University of Technology, Guangzhou, China. His main research interests are railway engineering, train operation optimization, energy-saving strategies in transportation and smart transportation.

**Bin Xu** received BEng in Electrical and Electronic Engineering from University of Liverpool, UK in 2020. He is currently a pre-enrolled master student in the School of Electrical and Computer Engineering, Cornell University, USA. He also works as a research assistant in the Department of Electrical and Electronic Engineering, Xi'an Jiaotong-Liverpool University, Suzhou, P.R. China. His research interests include railway energy-saving strategies, energy storage device and railway signaling system.

**Shaofeng Lu** is currently an associate professor with the Shien-Ming Wu School of Intelligent Engineering (WUSIE), South China University of Technology (SCUT), China. Before joining SCUT in 2019, he spent 6 years as a faculty member with Department of Electrical and Electronic Engineering, Xi'an Jiaotong-Liverpool University (XJTLU), China. He received the BEng and PhD degree from the University of Birmingham in 2007 and 2011 respectively. He also has a BEng degree from Huazhong University of Science and Technology, Wuhan, China. All are in Electrical and Electronic Engineering. His main research interests include power management strategies, railway traction system, electric vehicles, optimization techniques and energy-efficient transportation systems.

**Fei Xue** was born in 1977 in Tonghua of Jilin province in China. He received his Bachelor and Master degrees in power system and its automation from Wuhan University in China in 1999 and 2002, respectively. He received the Ph.D. of Electrical Engineering degree from the Department of Electrical Engineering of Politecnico di Torino, Torino, Italy, 2009. He was the Deputy Chief Engineer of Beijing XJ Electric Co.,Ltd and Lead Research Scientist in Siemens Eco-City Innovation Technologies (Tianjin) Co., Ltd. He is currently an associate professor with the Department of Electrical and Electronic Engineering, Xi'an Jiaotong-Liverpool University, No. 111 Ren'ai Road, Suzhou Industrial Park, Suzhou, P.R. China. His research interest focuses on power system security, integration of wind power into power grids, electric vehicle and energy internet.

**Lin Jiang** received the B.Sc. and M.Sc. degrees in electrical engineering from the Huazhong University of Science and Technology, Wuhan, China, and the Ph.D. degree in electrical engineering from the University of Liverpool, Liverpool, U.K., in 1992, 1996, and 2001, respectively. He was a Post-Doctoral Research Assistant with the University of Liverpool from 2001 to 2003 and a Post-Doctoral Research Associate with the Department of Automatic Control and Systems Engineering, University of Sheffield, Sheffield, U.K., from 2003 to 2005. He was a Senior Lecturer with the University of Glamorgan, Wales, U.K., from 2005 to 2007, and joined the University of Liverpool in 2007. He is currently a Senior Lecturer with the Department of Electrical Engineering and Electronics, University of Liverpool. His current research interests include control and analysis of power system, smart grid, and renewable energy.

**Minwu Chen** received the B.Eng. and Ph.D. degrees in electrical engineering from Southwest Jiaotong University, Chengdu, China, in 2004 and 2009, respectively. From 2010 to 2012, he undertook postdoctoral researches in the China Railway First Survey and Design Institute Group, Xi'an, China. Since 2018, he has been a Full Professor at the School of Electrical Engineering, Southwest Jiaotong University, Chengdu, China. From 2014 to 2015, he was a Visiting Scholar at the University of Birmingham, Birmingham, UK. His research interests include new technology and power quality for railway traction systems.